PLOS ONE

RESEARCH ARTICLE

MgO nanoparticles coated with polyethylene glycol as carrier for 2-Methoxyestradiol anticancer drug

Aline Alfaro[1,2☯], Andrea León[2,3☯], Emanuel Guajardo-Correa[1,2], Patricia Reúquen[1,2], Francisco Torres[4], Mario Mery[5], Rodrigo Segura[6], Paula A. Zapata[7], Pedro A. Orihuela[1,2]*

1 Laboratorio de Inmunología de la Reproducción, Facultad de Química y Biología, Universidad de Santiago de Chile, Santiago, Chile, **2** Centro para el Desarrollo de la Nanociencia y la Nanotecnología CEDENNA, Santiago, Chile, **3** Max Planck Institute for Chemical Physics of Solids, D-01068 Dresden, Germany, **4** Departamento de Física, Facultad de Ciencias Naturales, Universidad de Atacama, Copayapu 485, Copiapó, Chile, **5** Centro Científico Tecnológico de Valparaíso-CCTVal, Universidad Técnica Federico Santa María, Valparaíso, Chile, **6** Instituto de Química y Bioquímica, Facultad de Ciencias, Universidad de Valparaíso, Valparaíso, Chile, **7** Grupo Polímeros, Facultad de Química Biología, Universidad de Santiago de Chile, Santiago, Chile

☯ These authors contributed equally to this work.
* pedro.orihuela@usach.cl

Check for updates

OPEN ACCESS

Citation: Alfaro A, León A, Guajardo-Correa E, Reúquen P, Torres F, Mery M, et al. (2019) MgO nanoparticles coated with polyethylene glycol as carrier for 2-Methoxyestradiol anticancer drug. PLoS ONE 14(8): e0214900. https://doi.org/10.1371/journal.pone.0214900

Editor: Yogendra Kumar Mishra, Institute of Materials Science, GERMANY

Received: March 18, 2019

Accepted: June 21, 2019

Published: August 15, 2019

Copyright: © 2019 Alfaro et al. This is an open access article distributed under the terms of the Creative Commons Attribution License, which permits unrestricted use, distribution, and reproduction in any medium, provided the original author and source are credited.

Data Availability Statement: All relevant data are within the paper and its Supporting Information files.

Funding: This work received financial support from grants DICYT 021743OD-DAS and Basal Program for Centers of Excellence, Grant FB0807 CEDENNA, CONICYT and the DGIIP-USM. Proyecto Basal FB0821 – CONICYT. P.A. Zapata acknowledges the financial support of FONDECYT Regular N 1170226. A. León acknowledges the financial

Abstract

Novel Magnesium Oxide (MgO) nanoparticles (NPs) modified with the polymer polyethylene glycol (PEG) were synthesized as carrier for the anticancer drug 2-Methoxyestradiol (2ME) to improve its clinical application. The functionalized NPs were characterized by Infrared spectroscopy with Fourier transform to elucidate the vibration modes of this conjugate, indicating the formation of the MgO-PEG-2ME nanocomposite. The studies of absorption and liberation determined that MgO-PEG-2ME NPs incorporated 98.51 % of 2ME while liberation of 2ME was constant during 7 days at pH 2, 5 and 7.35. Finally, the MgO-PEG-2ME NPs decreased the viability of the prostate cancer cell line LNCap suggesting that this nanocomposite is suitable as a drug delivery system for anticancer prostate therapy.

Introduction

Cancer is one of the diseases with higher prevalence in the population, being the second cause of death in 2015, with a total of 8.8 million globally. It is expected that due to the growth and aging of the population in the next two decades 22 million of people will be diagnosed annually with this pathology [1, 2]. At global level the most common kinds of cancer are; lung, breast, duodenum and prostate [2, 3]. Prostate cancer is the most common type of carcinoma in male from developed and developing countries [4]. The current therapies for prostate cancer are focused in surgery, radiation and hormonal treatment. Unfortunately, survival prognostic for patients is very poor because many patients will suffer from recurrence and subsequent metastasis [4–6]. Therefore, it is necessary development new drugs and therapies that will be effective for the treatment of prostate cancer.

support of CONICYT Becas Chile Postdoctorado Grant No. 74190099.

Competing interests: The authors have declared that no competing interests exist.

2-Metoxyestradiol (2ME) has antitumor activity in several types of cancer of the reproductive tract as prostate, cervix, ovary or endometrium. 2ME exerts its anticancer activity via antiproliferative, apoptotic or antiangiogenic effects on tumor cells [7, 8]. Despite to be considerate as a promising anticancer drug it has an unfavorable kinetic with a low solubility in water; it is rapidly eliminated and has a low bioavailability because it quickly undergoes glucuronidations or other modifications [9]. Thus, it is necessary to find new ways to facilitate its administration to the human body. In this context, the nanoparticles (NPs) as drug carriers can play a fundamental role to improvement biological parameters without altering the anticancer properties of the drug. Actually, it has been proposed that polymeric NPs [10] or TiO_2 NPs coated with polyethylene glycol (PEG) could be useful tools to load 2ME [11]. In the searching for new NPs suitable for medical use, MgO NPs have been used as potential candidates because are biodegradable, biocompatible and non-toxic for a variety of human cell lines at concentrations under 300 μg/ml [12] which favors their use in biomedical applications [13]. On the other hand, MgO NPs are also used as carrier for anticancer drug such as; albumin and doxorubicin indicating its utility for a controlled system of drugs delivery [14–16]. Recently works have reported that MgO NPs and Nanoflkes as novel materials for doxorubicin loading [17].

Motivated by previous result made in MgO as NPs, we investigate the potential application of MgO NPs as carrier for 2ME. In this work, we first performed the physicochemical characterization of MgO NPs coated with PEG and loaded with 2ME (MgO-PEG-2ME). The efficiency of absorption and liberation of 2ME was then analyzed. Finally, the effect of MgO-PEG-2ME NPs on the prostate cell line LnCap was assessed.

Materials and methods

Synthesis of MgO nanoparticles

The MgO NPs were obtained by the sol-gel method [18] route assisted with cetyltrimethyl ammonium bromide $C_{19}H_42BrN$ (CTAB) as a surfactant to reduce the agglomeration of the NPs [19]. 1:1 molar solution of magnesium acetate, $Mg(CH_3COO)_2$ $4H_2O$ (99,5 %, MERK, USA) and tartaric acid $C_4H_6O_6$ to (99,5 %, MERK, USA) was prepared in ethanol and added dropwise over 10 ml of a 0.001 M of CTAB in water at 60˚C. The solution was stirred vigorously for 20 hours to achieve gel formation. Once the gel is formed, it was dried and before calcined at 600˚C for 6 hours to give MgO. The process of synthesis and characterization has been previously described [19].

MgO nanoparticles functionalized with PEG and 2ME loading

MgO NPs were covered with polyethylene glycol 600 (PEG600; Sigma Aldrich) using the agitation method. For this, 50 mg of MgO NPs were dispersed on 50 ml MiliQ water and stirred for 1 hour, then 88 μl of PEG 2mg/ml (The 88 μl correspond to necessary volume for obtain a 100 mg considering the PEG density) was added and stirred by 2 hours and centrifuged for 30 minutes at 4500 *g* (*g* is the gravity acceleration). The supernatant was discarded and the solid phase was dried on a heat plate (Memmert, Germany) at 60˚C. Then, 2ME 1 mg was added to 1 mg of MgO-PEG NPs and stirred for 2 hours and centrifuged at 10.621 *g* for 1 hour at 10˚C. Then, the solid phase was rinsed and dried on a heater plate (Memmert, Germany) at 60˚C.

Characterization techniques

The morphology and size of the NPs were determined by Transmission Electron Microscopy (TEM). The NPs were supported in a copper mesh covered with carbon (Support Films, Carbon Type-B, Ted Pella, inc.). The observations were performed with a TEM HT7700 (Hitashi,

Japan) at an acceleration voltage of 80 kV. The mean diameter particle of the NPs was obtained measuring at least 120 particles using the ImageJ software (National Institute of Health, USA). The functionalization of MgO-NPs by PEG and conjugation with 2ME were examined by Attenuated Total Reflectance Infrared Fourier-transform (FTIR) spectroscopy (ATR-FTIR). The FTIR spectra was collected in the 4000-1000 cm^{-1} range, with a resolution of 4 cm^{-1} at room temperature by using a Thermo Nicolet IS10 spectrometer provided with single bounce Ge crystal Smart-iTR accessory.

Zeta potential. Zeta potential was made in DMEM culture medium without supplementation and in phosphate buffer in order to mimic the size of the NPs at the time of performing the in vitro viability tests and to approximate the size that these NPs could have in blood circulation. No significant differences were found between DMEM and phosphate buffer. Therefore, the results shown in the manuscript were performed with phosphate buffer. Preparations were dissolved in 1 ml phosphate buffered saline at pH 7.35. The Samples were evaluated in triplicate. The zeta potential was analyzed by dynamic light scattering in the Zetasizer Nano ZS DST1070 cell (Malvern Instruments, UK) [20].

Ultra-high performance liquid chromatography (UPLC). UPLC was performed using an Acquity system (Waters, Milford, MA, USA) equipped with a binary solvent delivery pump, an autosampler and a tunable UV detector. Chromatographic separation was performed using a Waters Acquity BEH C18 column (50 × 2.1 mm, 1.7 mm). The mobile phase was a 70:30 (v:v) mixture of methanol and water at a flow rate of 0.4 ml/min. Detection was performed at a wavelength of 290 nm using a 10 μl injection volume; the mobile phase of water and methanol was maintained at 27˚C. The internal chromatographic standard solutions (1, 5, 10, 50 and 100 mg/ml) were freshly prepared in a volumetric flask along with the mobile phase [21].

Efficiency of absorption and liberation

The 2ME entrapment efficiency was analyzed using an extraction method described in our previously word [11]. 1 mg of MgO-PEG-2ME NPs was dispersed in 1 ml PBS, and agitation on an orbital shaker at 100 rpm. Samples were taken at 5 min, 30 min, 1 hour, 3 and 6 hours at 37˚C. The 2ME concentration was determined by UPLC using a calibration curve. To measure 2ME release, 1 mg of MgO-PEG-2ME NPs underwent rapid equilibrium dialysis (Thermo Scientific, see manufacturers instructions) through sequential bag dialysis at 37˚C with gentle shaking in 15 ml of PBS (pH 2, 5 and 7.35). At each sampling time, 1 ml of the supernatant was removed and replaced with an equivalent volume of PBS. The supernatants were analyzed by UPLC to determine 2ME release.

Cell culture. LNCap cells were grown in DMEM medium (Hyclone, USA) supplemented with sodium pyruvate 1 mM, 10% heat-inactivated fetal bovine serum, 100 UI/ml penicillin, 100 μg/ml streptomycin under 5% CO_2 in 95% of air in a cell culture incubator at 37˚C. The cells were used when reach to 70-80 % of confluency. For all experiments, 2.5×10^3 cells/well were seeded.

Treatments and measurement of cell viability. LNCaP cells were treated with nanoparticles of MgO, MgO-PEG or MgO-PEG- 2ME at a concentration equivalent to 5 μM of 2ME. The cell viability was assessed by the viability assays 3-(4,5-dimetiltiazol-2-il)- 5-(3-carboximetoxifenil)-2-(4-sulfofenil)- 2H-tetrazolio (MTS) using the Cell-Titer 96^c AQueous Non-Radioactive Cell Proliferation Assay kit (Promega, Madison, USA) according to manufacturer's instructions. LNCaP cells were grown on 96-well assay plates and 24, 48 or 72 hours post-treatment, 20 μl of MTS reagent provided by the kit was added to each well. After incubation, the absorbance value at 490 nm was obtained using an ELISA plate reader (Tecan Group Ltd.

Mnnedorf, Switzerland). As positive control of cytotoxicity we added hydrogen peroxide (H_2O_2) 0.08% dissolved in 4 μl of culture medium. Furthermore, as control we used a solution of 2ME 5 μM. Ethanol 0.01 % was used as vehicle of the nanoparticles and 2ME.

Statistical analysis. All relevant data are within the paper and its supporting information files. Data for cellular viability assays were performed in triplicate. The data were analyzed using GraphPad Prism (GraphPad Software, San Diego, CA, USA). When correspond, all data are presented as mean standard error. Overall analysis was done by Kruskal-Wallis test followed by Mann-Whitney U test for pair-wise comparisons when overall significance was detected. Differences were considered significant at $P < 0.05$.

Results and discussions

Characterization of MgO, MgO-PEG and MgO-PEG-2ME NPs

Figs 1 and 2 (see S1 Table) reveals that the MgO NPs are lightly agglomerated forming small particles in a narrow size distribution with a mean value of 15.7 ± 4.3 nm. When PEG and 2ME were add to MgO NPs, the size mean value increase with the size around 16.0 ± 10.6 nm (Figs 1B and 2) and 93.31 ± 74.0 nm (Figs 1C and 2) for MgO-PEG and MgO-PEG-2ME respectively. The histogram distribution for pure MgO-NPs, MgO-PEG and MgO-PEG-2ME is shown in the Fig 2.

The size of the NPs is an important parameter that determines his biocompatibility; our results for TEM analysis show a wide size distribution, which could be optimal for the internalization into the intracellular space [22] via different mechanisms as endocytosis, phagocytosis and pinocytosis. Particularly, endocytosis mediated by clathrin and caveolae induce a greater accumulation of NPs inside the cells [23]. In addition, it must be considered that for each NPs that is able to be transported across the cell membrane exist an ideal radius that allows a rapid internalization. As this radius is approximately 90 nm for spherical conjugate NPs, we can assume that our NPs are suitable for cell internalization [24]. Other variables that determine the biocompatibility of the NPs is the superficial charge due to chemistry modification. The results of the zeta potential measurements for MgO, MgO-PEG and MgO-PEG-2ME NPs are shown in the Table 1. We can observe a negative zeta potential increasing from -30 meV to -28.3 and -22.0 when PEG and 2ME are added suggesting that these NPs could be useful for biological applications. In this context, It has been shown that NPs with positive zeta potential could be more deleterious because induce platelet aggregation that can cause thrombosis or they can interact with membrane phospholipid or proteins disrupting stability of the cell surface [24].

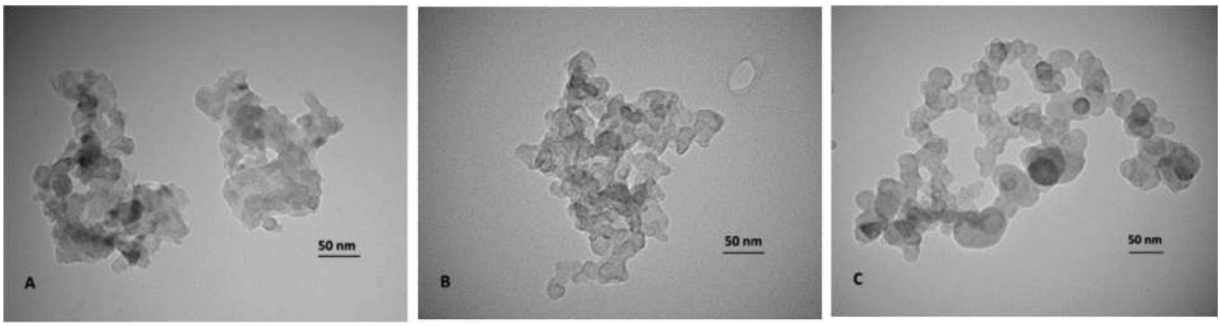

Fig 1. Nanoparticles photomicrographs. Representative nanoparticles photomicrographs: (A) MgO, (B) MgO-PEG and (C) MgO-PEG-2ME. Note that MgO-PEG-2ME are bigger than other nanoparticles.

https://doi.org/10.1371/journal.pone.0214900.g001

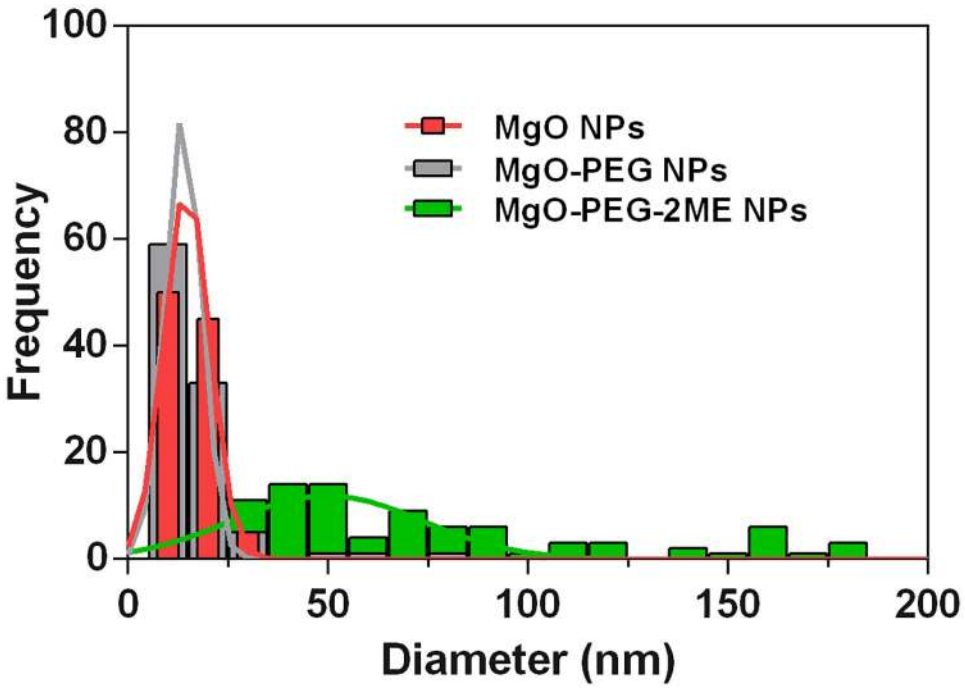

Fig 2. Histogram. Histogram distribution of the MgO, MgO-PEG and MgO-PEG-2ME NPs.

https://doi.org/10.1371/journal.pone.0214900.g002

To characterize and determine functional groups and modifications, FTIR spectroscopy was performed on pure MgO-NPs, PEG and 2ME as well as in MgO-PEG, MgO-PEG-2ME NPs and PEG-2ME. Fig 3A shows the spectrum of the MgO, PEG, MgO-PEG, MgO-PEG-2ME. For MgO, three principal bands are found; at 3700 cm^{-1} belong to the O-H group, at 1400 cm^{-1} corresponding to Mg-O stretching vibration [15, 25] and at 846 cm^{-1} which has been attributed to the formation of cubic phase of MgO [25]. The FTIR PEG shows the characteristic bands at 2929 cm^{-1}, 2888 cm^{-1}, 1342 cm^{-1}, 1242 cm^{-1} and 1100 cm^{-1} that have been described by [26, 27]. When PEG is added to NPs we can observe that the bands are modified, with respect to pure MgO-NPs mainly at 1098 cm^{-1} (C-O stretching vibration) [25], this band is shifted at 1081 cm^{-1} from their original position in pure PEG, exhibiting hydrogen-bonding nature and suggests that PEG interaction with the surface of MgO-NPs [25]. The FTIR spectrum of pure 2ME exhibit characteristic bands occurring at 3417 cm^{-1}, 3182 cm^{-1}, 3000 cm^{-1}, 2963 cm^{-1}, 2907 cm^{-1}, 2809 cm^{-1}, and 1600 cm^{-1}, and also in the ranges between 1500-1400 cm^{-1} and 1300-1000 cm^{-1}, the last bands are the fingerprint of 2ME, that have been described previously by our research group [11].

In the FTIR spectrum of MgO-PEG-2ME NPs, we found several changes including new bands at 2861 cm^{-1} and 2919 cm^{-1} belonging the C-H stretching vibration in CH, $-CH_2$,

Table 1. Mean ± zeta potential.

NPs	Zeta Potential (mV)
MgO	-30.7 ± 0.6
MgO-PEG	-28.3 ± 3.5
MgO-PEG-2ME	-22.0 ± 10.8

Mean ± Zeta Potential for Nanoparticles of MgO, MgO-PEG and MgO-PEG-2ME NPs.

https://doi.org/10.1371/journal.pone.0214900.t001

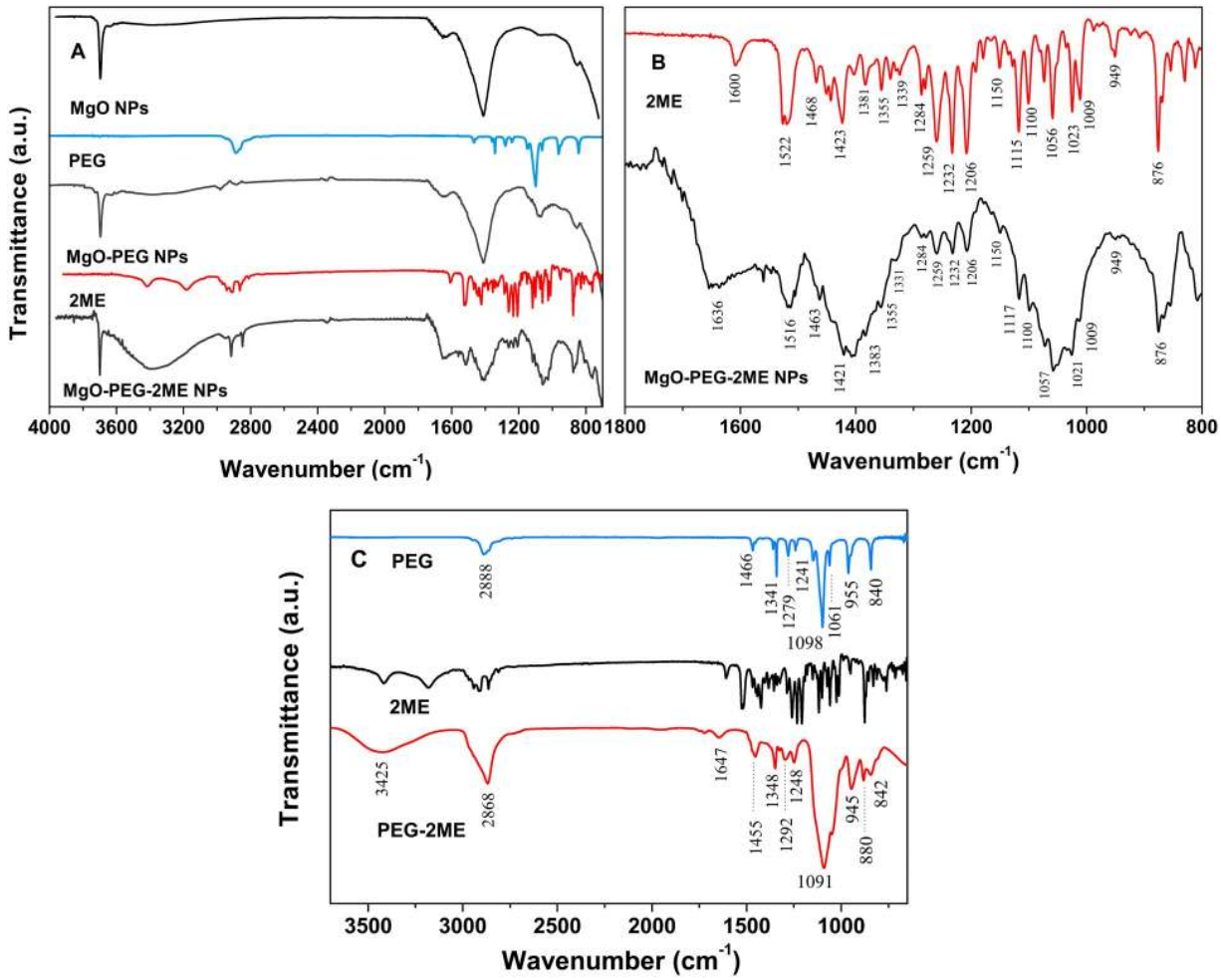

Fig 3. Fourier-Transform Infrared (FTIR) spectra. (A) Fourier-transform infrared (FTIR) spectra for: MgO, PEG, MgO-PEG, 2ME, and MgO-PEG-2ME. (B) 2ME and MgO-PEG-2ME NPs spectra in the range of [1800-800 cm^{-1}]. In this zone we can distinguish the principal functional groups of 2ME and the new bands that appear in MgO-PEG when is conjugate with 2ME, where the mains bands are labeled. (C) PEG, 2ME and PEG-2ME; this figure shows the modified band of PEG when is conjugate with 2ME, where the mains bands are labeled.

https://doi.org/10.1371/journal.pone.0214900.g003

-CH_3. The band at 3382 cm^{-1} is related with the stretching vibration of hydroxyl group, this band is broadened with an increased intensity with respect to pure 2ME. The band localized between 1500-1460 cm^{-1} are attributed to bending modes of CH, -CH_2, -CH_3 that overlap with Mg-O vibration of MgO NPs given as result a decreased intensity band with respect to pure MgO. On the other hand, new bands belonging to 2ME are observed mainly at 1259 cm^{-1}, 1231 cm^{-1} and 1206 cm^{-1}, these peaks corresponding to the methoxy group O-CH_3 and hydroxyl group C-OH from 2ME. Finally, in the low frequency vibration of 1179-638 cm^{-1} several bands are overlapping between 2ME and MgO-PEG which generate broader bands compared with MgO-PEG NPs. The appearance of the characteristics bands of 2ME slightly shifted when 2ME is conjugated with MgO-PEG (see Fig 3B in the range 1600-800 cm^{-1}). This suggests that the interaction of 2ME and PEG may occur through hydrogen bondings of the hydroxyl groups present on the MgO-PEG surface. Furthermore, it is known that PEG is not a purely hydrophilic polymer, being able to attach hydrophobic drug as 2ME [28, 29]. For corroborate this, we perform the spectra of PEG conjugated with 2ME without MgO-NPs, this is shown in the Fig 3C. In this figure we can observe that the PEG-2ME bands are modified with

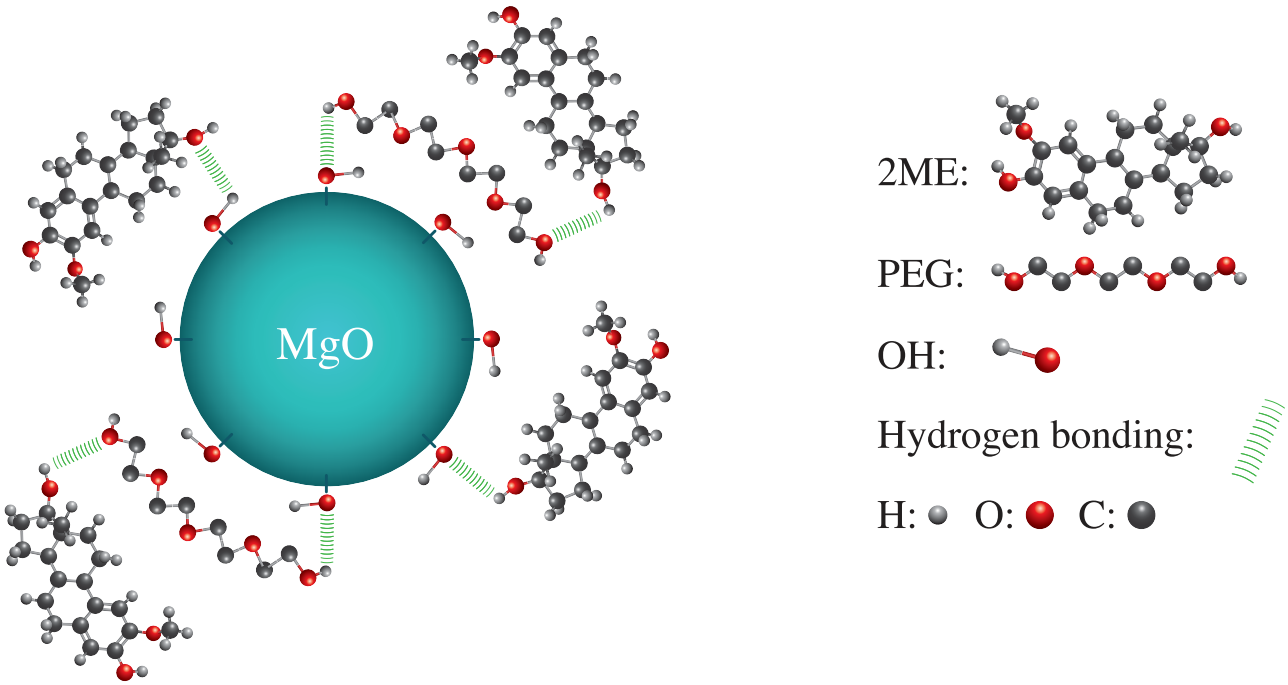

Fig 4. Schematic representation. Schematic representation of MgO NPs conjugate with PEG and 2ME. This figure shows a representation of the interaction between MgO-PEG, MgO-2ME and PEG-2ME. The Green lines represent the hydrogen bonding between OH group of PEG and 2ME molecules with OH groups of MgO NPs. The color of spheres (light gray, red and gray) represent Hydrogen (H), Oxygen (O) and Carbon (C).

https://doi.org/10.1371/journal.pone.0214900.g004

respect to PEG and 2ME alone; the most striking feature of PEG-2ME spectra is that, the bands became wider than PEG bands, this may be originated from the association between OH group of PEG and hydroxyl group of 2ME by hydrogen bonding. All these characteristic and those exposed above indicate the attachment of 2ME to MgO-PEG NPs. A scheme of functionalized MgO Nps with PEG and 2ME is shown in the Fig 4. All relevant FTIR data is supported by S2 Table.

Kinetic of absorption and liberation

To evaluate the 2ME-loading capacity of the MgO-PEG NPs, we performed an extraction method in which an amount (i.e., 1 mg) of particles was dispersed in water to release the encapsulated drug, and this solution was evaporated and subsequently suspended in methanol for quantification by UPLC. The maximum absorption was reached at 3 hours of incubation with a value of 0.985 ± 0.0011 mg/ml of 2ME absorbed by each 1 mg/ml of MgO-PEG NPs that correspond to 98.51 % of absorption of total weight; this amount keeps stable until 6 hours of evaluation (see Fig 5 and S3 Table).

As the retention of the chemotherapeutic drug within the nanoparticle is fundamental for its future clinical application, we then measured the liberation of 2ME from the MgO-PEG NPs in non-biological conditions. As shown in Fig 6 and S4 Table, we can observe that 2ME is gradually released over a period of 168 hours (7 days at pH 2, 5 and 7.35). This shows that the drug is released in a sustained manner. The mean value of release is about 33.9 %, 28.39 % and 30.16 % at pH 2, 5 and 7.35, respectively. The maximum amount released is 2.95 μM that correspond to 89.27 % of the total of 2ME loaded into MgO-PEG NPs, which is reached for a pH 5 at 96 hours. For a pH 7.35, the maximum drug released was 44 % at 72 hours. These results suggest a high specificity for any potential future use of this nanoparticles since less than 1% of

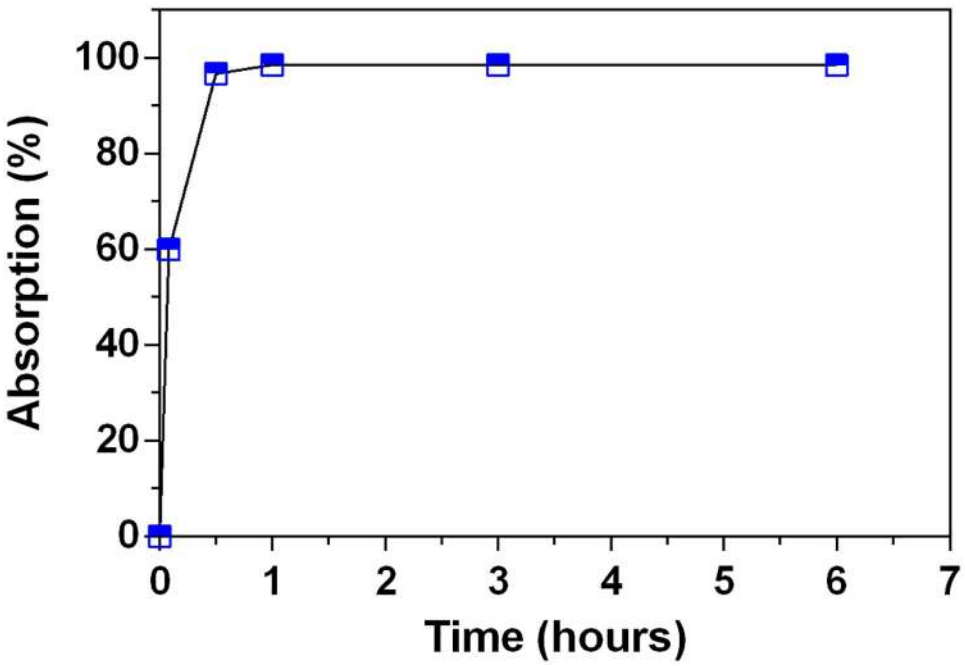

Fig 5. Absorption profile of 2ME by MgO-PEG NPs.

https://doi.org/10.1371/journal.pone.0214900.g005

2ME would be released into the circulation, and given the leaky blood vasculature that irrigates cancer cells the MgO-PEG-2ME composite should be taken up preferentially.

Cell toxicity

Viability of LnCap cells treated with MgO NPs, MgO-PEG NPs, MgO-PEG- 2ME NPs at a concentration equivalent to 5 μM of 2ME were determined using an in vitro viability assays (MTS). As shown in Fig 7 and S5 Table, 2ME alone or loaded to MgO-PEG NPs induce a significant decrease in cell viability around 40% at 72 hours. These results indicate that 2ME absorbed with the MgO-PEG NPs maintains its anticancer properties suggesting that this conjugate is a promising option for therapeutic use. The NPs were loaded with a concentration of 2ME necessary to reach 5 μM which is the higher therapeutics dose; however, previous reports have shown that 2ME could affect cell viability in a range of dose between 0.08-5 μM [9] so

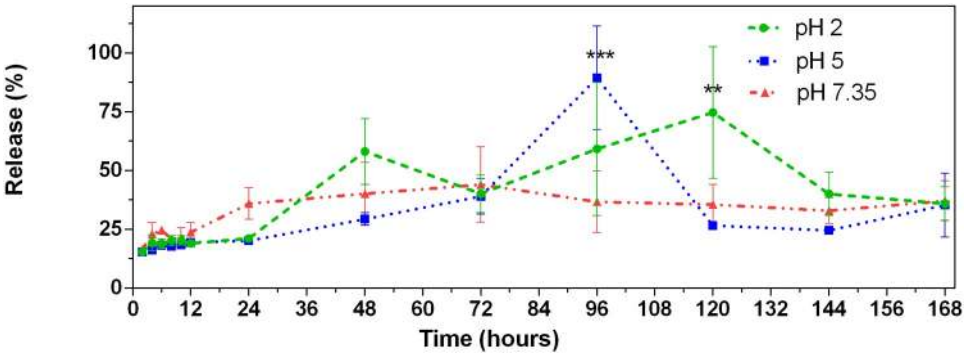

Fig 6. Release profile drug. 2ME release profile in % from functionalized MgO-PEG NPs, ** $P < 0.01$, *** $P < 0.001$.

https://doi.org/10.1371/journal.pone.0214900.g006

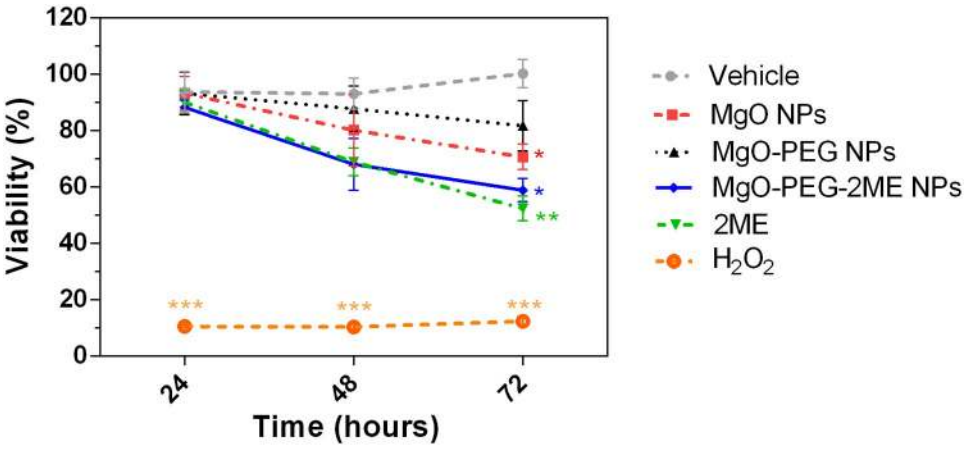

Fig 7. Cell viability. Viability of LNCaP cells treated for 24, 48 or 72 hours with nanoparticles of MgO, MgO-PEG, or MgO-PEG-2ME compared with 2ME 5 μM alone. Ethanol 0.01% was used as Vehicle of the nanoparticles and 2ME. As positive control of cytotoxicity we added hydrogen peroxide (H_2O_2) 0.08 % dissolved in 4 μL of culture medium, $^{*}P < 0.05$, $^{**}P < 0.01$, $^{***}P < 0.001$.

https://doi.org/10.1371/journal.pone.0214900.g007

that it is probable that the LnCap cells only need a low concentration of 2ME. Interestingly, we also observed that pure MgO-NPs produce a significant decrease in the cell viability to 20% at 72 hours, which decreases when it is coated with PEG suggesting that functionalization of MgO NPs with PEG reduces its intrinsic toxicity. This is may be explained by the fact that PEG inhibit protein absorption and/or reduce surface availability of NPs affecting their toxic activity [23, 26, 30]. On the other hand, it has been reported that 2ME has an anticancer effect based on its antiproliferative, proapoptotic and antiangiogenic activities [7, 8]. Based in these previous studies, we performed the viability assay to demonstrate that MgO-PEG-2ME NPs has proapoptotic action as described for the 2ME alone; we think that this work can be a motivation for futures works focused in the evaluation of the anti-angiogenic and antiproliferative action of the drug and perform other tests such as ROS analysis.

Conclusion

Nanoparticles of MgO, MgO-PEG and MgO-PEG-2ME were characterized by TEM, zeta potential and FTIR spectroscopy. The modification processes attributed to the conjugation of PEG and 2ME into MgO NPs was performed step by step, where is confirmed that 2ME is attached to functionalized MgO-PEG NPs. The 2ME absorption profile shows that a 98.51% of total weight is absorbed by MgO-PEG NPs. 2ME is released from MgO-PEG NPs constantly over a period time reaching a maximum of 2.95 μM at 96 hrs corresponding to 89.27 % of the 2ME total loaded into MgO-PEG NPs. In vitro viability assays (MTS) with the human prostatic adenocarcinoma cell line LNCap showed that MgO-PEG-2ME NPs has anticancer activity as similar as 2ME alone. In summary, we have developed a nanocarrier system based in MgO--PEG NPs that can load and deliver 2ME into cancer cells suggesting to this 2ME loading strategy as a promising option for use in malignant disease.

Supporting information

S1 Table. Raw data for histogram distribution of the MgO, MgO-PEG and MgO-PEG-2ME NPs.
(XLSX)

S2 Table. Raw data for the Fourier-Transform Infrared (FTIR) spectra.
(XLSX)

S3 Table. Raw data for the absorption profile of 2ME by MgO-PEG NPs.
(XLSX)

S4 Table. Raw data for the release profile 2ME.
(XLSX)

S5 Table. Raw data for cell viability.
(XLSX)

Acknowledgments

This work received financial support from grants DICYT 021743OD-DAS and Basal Program for Centers of Excellence, Grant FB0807 CEDENNA, Proyecto Basal FB0821–CONICYT. P.A. Zapata acknowledges the financial support of FONDECYT Regular No. 1170226. A. León acknowledges the financial support of CONICYT Becas Chile Postdoctorado Grant No. 74190099.

Author Contributions

Conceptualization: Andrea León.

Data curation: Aline Alfaro.

Formal analysis: Aline Alfaro, Andrea León, Patricia Reúquen, Francisco Torres, Mario Mery, Paula A. Zapata, Pedro A. Orihuela.

Funding acquisition: Pedro A. Orihuela.

Investigation: Aline Alfaro, Andrea León, Patricia Reúquen, Francisco Torres, Pedro A. Orihuela.

Methodology: Aline Alfaro, Andrea León, Emanuel Guajardo-Correa, Mario Mery, Rodrigo Segura, Paula A. Zapata, Pedro A. Orihuela.

Project administration: Andrea León, Pedro A. Orihuela.

Resources: Andrea León, Emanuel Guajardo-Correa, Rodrigo Segura, Paula A. Zapata, Pedro A. Orihuela.

Software: Aline Alfaro, Andrea León, Mario Mery, Rodrigo Segura.

Supervision: Andrea León, Patricia Reúquen, Paula A. Zapata, Pedro A. Orihuela.

Validation: Andrea León, Rodrigo Segura, Paula A. Zapata, Pedro A. Orihuela.

Visualization: Andrea León, Mario Mery, Pedro A. Orihuela.

Writing – original draft: Andrea León, Patricia Reúquen, Francisco Torres.

Writing – review & editing: Andrea León, Pedro A. Orihuela.

References

1. Haume K, Rosa S, Grellet S, Śmiałek MA, Butterworth KT, Solov'yov AV., et al. Gold nanoparticles for cancer radiotherapy: a review. Cancer Nanotechnol. 2016; 7(1): 8. https://doi.org/10.1186/s12645-016-0021-x

2. Jemal A, Center MM, DeSantis C, Ward EM. Global patterns of cancer incidence and mortality rates and trends. Cancer Epidemiol Biomarkers Prev. 2010; 19(8): 1893–907. https://doi.org/10.1158/1055-9965.EPI-10-0437
3. Saslow D, Boetes C, Burke W, Harms S, Leach MO, Lehman CD, et al. American Cancer Society guidelines for breast screening with MRI as an adjunct to mammography. CA Cancer J Clin. 2007; 57 (2): 75–89. https://doi.org/10.3322/canjclin.57.2.75 PMID: 17392385
4. Chang AJ, Autio KA, Roach M III, Scher HI. High-risk prostate cancer-classification and therapy. Nat Rev Clin Oncol. 2014; 11(6): 308–23. https://doi.org/10.1038/nrclinonc.2014.68 PMID: 24840073
5. Lowes LE, Lock M, Rodrigues G, D'Souza D, Bauman G, Ahmad B, et al. The significance of circulating tumor cells in prostate cancer patients undergoing adjuvant or salvage radiation therapy. Prostate Cancer Prostatic Dis. 2015; 18(4): 358–64. https://doi.org/10.1038/pcan.2015.36 PMID: 26238233
6. Welch HG, Gorski DH, Albertsen PC. Trends in metastatic breast and prostate cancer—lessons in cancer dynamics. N Engl J Med. 2015; 373(18): 1685–7. https://doi.org/10.1056/NEJMp1510443 PMID: 26510017
7. Mueck AO and Seeger H.2-Methoxyestradiol—biology and mechanism of action Steroids. 2010; 75 (10): 625–31. https://doi.org/10.1016/j.steroids.2010.02.016 PMID: 20214913
8. Ireson CR, Chander SK, Purohit A, Perera S, Newman SP, Parish D, et al. Pharmacokinetics and efficacy of 2-methoxyoestradiol and 2-methoxyoestradiol-bis-sulphamate in vivo in rodents. Br J Cancer. 2004; 90(4): 932–7. https://doi.org/10.1038/sj.bjc.6601591 PMID: 14970876
9. Verenich S, Gerk PM. Therapeutic promises of 2-methoxyestradiol and its drug disposition challenges, Mol Pharm. 2010; 7(6): 2030–9. https://doi.org/10.1021/mp100190f PMID: 20831190
10. Wang Y, Guo R, Cao X, Shen M, Shi X. Encapsulation of 2-methoxyestradiol within multifunctional poly (amidoamine) dendrimers for targeted cancer therapy. Biomaterials. 2011; 32(12): 3322–9. https://doi.org/10.1016/j.biomaterials.2010.12.060 PMID: 21315444
11. León A, Reuquen P, Garín C, Segura R, Vargas P, Zapata P, et al. FTIR and Raman characterization of TiO_2 nanoparticles coated with polyethylene glycol as carrier for 2-methoxyestradiol. Applied Sciences. 2017; 7(1): 49. https://doi.org/10.3390/app7010049
12. Mahmoud A, Ezgi Ö, Merve A, Özhan G. In vitro toxicological assessment of magnesium oxide nanoparticle exposure in several mammalian cell types. Int J Toxicol. 2016; 35(4): 429–37. https://doi.org/10.1177/1091581816648624 PMID: 27177543
13. Di DR, He ZZ, Sun ZQ, Liu J. A new nano-cryosurgical modality for tumor treatment using biodegradable MgO nanoparticles. Nanomedicine. 2012; 8(8): 1233–41. https://doi.org/10.1016/j.nano.2012.02.010 PMID: 22406189
14. Behzadi E, Sarsharzadeh R, Nouri M, Attar F, Akhtari K, Shahpasand K, Falahati M. Albumin binding and anticancer effect of magnesium oxide nanoparticles. Int J Nanomedicine. 2018; 14: 257–270. https://doi.org/10.2147/IJN.S186428 PMID: 30643405
15. Somanathan T, Krishna VM, Saravanan V, Kumar R, Kumar R. MgO Nanoparticles for Effective Uptake and Release of Doxorubicin Drug: pH Sensitive Controlled Drug Release. J. Nanosci. Nanotechnol. 2016; 16(9): 9421–31. https://doi.org/10.1166/jnn.2016.12164
16. Kumar R, Gokulakrishnan N, Kumar R, Krishna VM, Saravanan A, Supriya S, et al. Can Be a Bimetal Oxide ZnO—MgO Nanoparticles Anticancer Drug Carrier and Deliver? Doxorubicin Adsorption/Release Study. J Nanosci Nanotechnol. 2015; 15(2): 1543–53. https://doi.org/10.1166/jnn.2015.8915 PMID: 26353689
17. Ranathunge TA, Karunaratne DGGP, Rajapakse RMG, Watkins DL. Doxorubicin Loaded Magnesium Oxide Nanoflakes as pH Dependent Carriers for Simultaneous Treatment of Cancer and Hypomagnesemia. Nanomaterials. 2019; 9(2). https://doi.org/10.3390/nano9020208 PMID: 30736270
18. Tang ZX, Lv BF. MgO nanoparticles as antibacterial agent: preparation and activity. Braz J Chem Eng. 2014; 31(3): 591–601. https://doi.org/10.1590/0104-6632.20140313s00002813
19. Mastuli MS, Ansari NS, Nawawi MA, Mahat AM. Effects of cationic surfactant in sol-gel synthesis of nano sized magnesium oxide. APCBEE Proc. 2012; 3: 93–98. https://doi.org/10.1016/j.apcbee.2012.06.052
20. Vilos C, Morales FA, Solar PA, Herrera NS, Gonzalez-Nilo FD, Aguayo DA, et al. Paclitaxel-PHBV nanoparticles and their toxicity to endometrial and primary ovarian cancer cells. Biomaterials. 2013; 34 (16): 4098–4108. https://doi.org/10.1016/j.biomaterials.2013.02.034 PMID: 23465827
21. Wu Y, Engen JR, Hobbins WB. Ultra performance liquid chromatography (UPLC) further improves hydrogen/deuterium exchange mass spectrometry. J Control Release. 2014; 190: 485–99.
22. Yameen B, Choi WI, Vilos C, Swami A, Shi J, Farokhzad OC. Insight into nanoparticle cellular uptake and intracellular targeting. J Control Release. 2014; 190: 485–99. https://doi.org/10.1016/j.jconrel.2014.06.038 PMID: 24984011

23. Mano SS, Kanehira K, Sonezaki S, Taniguchi A. Effect of polyethylene glycol modification of TiO_2 nanoparticles on cytotoxicity and gene expressions in human cell lines. Int J Mol Sci. 2012; 13(3): 3703–17. https://doi.org/10.3390/ijms13033703 PMID: 22489177

24. Shi J, Kantoff PW, Wooster R, Farokhzad OC. Cancer nanomedicine: progress, challenges and opportunities. Nat Rev Cancer. 2017; 17(1): 20–37. https://doi.org/10.1038/nrc.2016.108 PMID: 27834398

25. Akram MW, Fakhar-e-Alam M, Atif M, Butt AR, Asghar A, Jamil Y, et al. In vitro evaluation of the toxic effects of MgO nanostructure in Hela cell line. Sci Rep. 2018; 8(1): 4576. https://doi.org/10.1038/s41598-018-23105-y PMID: 29545644

26. Venkatasubbu GD, Ramasamy S, Ramakrishnan V, Kumar J. Folate targeted PEGylated titanium dioxide nanoparticles as a nanocarrier for targeted paclitaxel drug delivery. Adv Powder Technol. 2013; 24 (6): 947–54. https://doi.org/10.1016/j.apt.2013.01.008

27. Naghibi S, Hosseini HR, Sani MA, Shokrgozar MA, Mehrjoo M. Mortality response of folate receptor-activated, PEG–functionalized TiO_2 nanoparticles for doxorubicin loading with and without ultraviolet irradiation. Ceram. Int. 2014; 40(4): 5481–8. https://doi.org/10.1016/j.ceramint.2013.10.136

28. Bunker A. Poly (ethylene glycol) in drug delivery, why does it work, and can we do better? All atom molecular dynamics simulation provides some answers. Phys. Proc. 2012; 34: 24–33. https://doi.org/10.1016/j.phpro.2012.05.004

29. Li YC, Rissanen S, Stepniewski M, Cramariuc O, Róg T, Mirza S, et al. Study of interaction between PEG carrier and three relevant drug molecules: piroxicam, paclitaxel, and hematoporphyrin. J. Phys. Chem. B. 2012; 116(24): 7334–41. https://doi.org/10.1021/jp300301z PMID: 22587534

30. Jokerst JV, Lobovkina T, Zare RN, Gambhir SS. Nanoparticle PEGylation for imaging and therapy. Nanomedicine (Lond). 2011; 6(4): 715–28. https://doi.org/10.2217/nnm.11.19